ACSNANO

www.acsnano.org

ARTICLE

Monodisperse Liposomes with Femtoliter Volume Enable Quantitative Digital Bioassays of Membrane Transporters and Cell-Free Gene Expression

Naoki Soga, Akira Ota, Kota Nakajima, Rikiya Watanabe, Hiroshi Ueno, and Hiroyuki Noji*

Cite This: *ACS Nano* 2020, 14, 11700−11711

Read Online

ACCESS | Metrics & More | Article Recommendations | Supporting Information

ABSTRACT: **Digital bioassays have emerged as a new category of bioanalysis. However, digital bioassays for membrane transporter proteins have not been well established yet despite high demands in molecular physiology and molecular pharmacology due to the lack of biologically functional monodisperse liposomes with femtoliter volumes. Here, we established a simple and robust method to produce femtoliter-sized liposomes (femto-liposomes). We prepared 10^6 monodispersed water-in-oil droplets stabilized by a lipid monolayer using a polyethylene glycol-coated femtoliter reactor array device. Droplets were subjected to the optimized emulsion transfer process for femto-liposome production. Liposomes were monodispersed (coefficient of variation = 5−15%) and had suitable diameter (0.6−5.3 μm) and uniform volumes of subfemtoliter or a few femtoliters; thus, they were termed uniform femto-liposomes. The unilamellarity of uniform femto-liposomes allowed quantitative single-molecule analysis of passive and active transporter proteins: α-hemolysin and F_oF_1-ATPase. Digital gene expression in uniform femto-liposomes (cell-free transcription and translation from single DNA molecules) was also demonstrated, showing the versatility of digital assays for membrane transporter proteins and cell-free synthetic biology.**

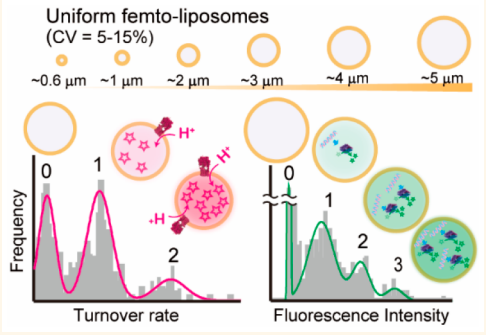

KEYWORDS: *liposome, digital bioassays, membrane transporter, cell-free gene expression, single-molecule analysis, microdevice*

Digital bioassays have emerged as a novel paradigm of bioanalytical strategy for highly sensitive and quantitative measurements.[1−3] This technology enables the quantification and detailed analysis of various kinds of biomolecules from nucleic acids and proteins to viruses at the single-molecule/particle level.[4−7] Thus, the representative class of digital bioassays, such as digital polymerase chain reaction (digital PCR)[8,9] and digital enzyme-linked immunosorbent assay (digital ELISA),[10,11] has already been commercialized as a next-generation platform for diagnostic tests. In a typical format of digital bioassays, each target molecule is stochastically encapsulated in microcompartments at the single-molecule level. Then, target molecules themselves or enzyme molecules bound to target molecules *via* a binder (e.g., antibodies) catalyze fluorogenic reactions, thereby producing fluorescence dye molecules. Due to the small volume, microcompartments encapsulating target molecules accumulate fluorescent dyes, yielding a detectable level of fluorescence signal in a short time (typically, a few minutes), while microcompartments with no target molecule remain dark. After the fluorescence signal is binarized, the total number of target molecules for the positive reactors can be counted.

Digital bioassays in the microcompartmentalization method have key technological features. First, microreactors have to be sufficient and suitably small to enrich the fluorescent reaction product within practical timeframes. In digital PCR or other detection methods producing signals *via* exponential amplification, relatively large reactors, 10−100 μm in diameter, are applicable for the assays. Smaller reactors, 10 μm or less, are required for enzyme-based digital assays such as digital ELISA, which amplify fluorescence signals monotonically with incubation time. The second requirement is uniformity in

Received: May 25, 2020
Accepted: August 13, 2020
Published: August 30, 2020

https://dx.doi.org/10.1021/acsnano.0c04354
ACS Nano 2020, 14, 11700−11711

reactor size. This is requisite for quantitative digital bioassays to ensure the equal probability of target encapsulation among reactors. Although one of the earliest single-molecule enzyme detection systems was achieved by partitioning β-galactosidase assay solution in water-in-oil emulsions in the 1960s,[12] quantitative analysis had to wait over 40 years until regularly shaped micron-sized reactors became available for single-molecule enzyme assays.[5] Subsequently, various microcompartmentalization techniques for digital bioassays have been explored, including microcavities on a glass gasket[4] or water-in-oil droplet array displayed on fabricated polymer sheet[13] or on a slipchip.[14] Freely suspended water-in-oil droplets generated with flow-focusing microchannel[15,16] and particle-based emulsification[17] are also used in digital bioassays, although many of them were used for DNA detection because of the relatively large size.

With the expansion of the microcompartmentalization technology, a variety of bioassays have also explored implementation in a digital format. Examples of digitized nucleic acid detection assays include PCR, loop-mediated isothermal amplification (LAMP),[18,19] and digital nucleic acid sequence-based amplification (NASBA).[20] Various fluorogenic enzyme assays have also been developed to expand the variety of enzymes and available colors for digital bioassays.[21−26] These are considered the basis for multiplex analyses for enzyme-based assays such as digital ELISA. Fluorogenic influenza virus detection was also digitized for highly sensitive detection.[7]

Thus, this field has been seeing considerable progress, expanding microcompartmentalization methods and biochemical wetwares. However, digital bioassays remain limited to water-soluble molecules and simple biochemical systems. For example, digital bioassays for membrane proteins are very few, despite the large demand for quantitative analysis of membrane proteins from molecular physiology and pharmacological studies.[27] To address this challenge, we developed arrayed lipid bilayer chamber systems (ALBiCs) based on the femtoliter reactor array device (FRAD) for quantitative digital bioassay for membrane transporter proteins.[28] Although it enables quantitative analysis of single transporter molecules like α-hemolysin, ATP synthase, and TMEM16F (a phospholipid scramblase),[29] the device surfaces of the microreactor device often cause nonspecific interaction and absorption of molecules.[28] We also explored the possibility of implementing more complex systems in a FRAD system: cell-free transcription and translation from single-molecule DNA (digital gene expression) was developed for highly accurate selection of clones encoding enzymes with enhanced catalytic activity.[30] However, these methods still have limitations when one aims to avoid nonspecific interaction of molecules with device surfaces or to reconstitute more dynamic systems accompanying morphological changes in membranes, like fusion, fission, budding, or division.[31]

A simple and fundamental solution for these problems is to use monodisperse liposomes as the microreactors. This is because the lipid bilayer of the liposome has the ideal surface for most biomolecules to avoid nonspecific absorption.[32] In addition, the lipid surface is reported to stimulize the assembly or aggregation of biomolecules such as amyloid formation.[33] Thus, monodisperse liposomes would be a platform allowing quantitative features of disease-related degeneration of biomolecules. Moreover, the lipid bilayer is physically flexible to show dynamic morphological changes under adequate stimuli. However, conventional methods for the preparation of liposomes—reverse-phase evaporation, electroformation, emulsion transfer or thin-film hydration methods—result in size polydispersity.[34] Although the size-extrusion process produces more uniform liposomes, the coefficient of variation in size still remained around 20−40%.[35] Furthermore, the size of the liposomes prepared with extruders is too small (in the range of 10−100 nm) for quantitative analysis under optical microscopy. For the production of monodisperse liposomes suitable for optical microscopic analysis, several types of microsystems have been reported, including flow-focus devices or pulsed jet flow systems.[36] These techniques realize the preparation of monodisperse liposomes with sufficiently low coefficient of variation (>4%). These liposomes prepared in such microsystems are typically 10 μm or larger,[37] too large for digital assays of membrane transporters. A few examples are found where liposomes smaller than 10 μm were prepared.[38−43] However, the biofunctionality of such liposomes was not tested, and single-molecule analysis was not explored.

Here, we present a simple and robust method to produce $>10^6$ small and monodispersed water-in-oil (w/o) droplets. The droplets were subjected to emulsion transfer to prepare monodisperse liposomes in a high-throughput manner. The generated liposomes displayed fine monodispersity, with a coefficient of variation as low as 5−15%, resulting in a uniform volume of subfemtoliter or a few femtoliters; these were termed uniform femto-liposomes. We also confirmed the functionality of the liposomes by testing the activity of transporter membrane proteins. Quantitative digital assays for passive and active transporter proteins, α-hemolysin and F_oF_1-ATPase, are demonstrated to emphasize the merit of the monodispersity of the uniform femto-liposomes. Finally, we demonstrate digital and cell-free gene expression from a single molecule of DNA in uniform femto-liposomes, showing the possibility to build more complex systems for cell-free synthetic biology research.

RESULTS AND DISCUSSION

Preparation of Monodisperse Droplets. For the production of monodisperse droplets with a diameter of 0.6−5.3 μm, we used a femtoliter reactor array device (FRAD) displaying micron-sized droplets, which has been used for single-molecule enzyme assays,[13] digital ELISA,[10] arrayed lipid bilayer systems,[28,29,44] and cell-free gene expression from a single DNA molecule (digital gene expression).[30] The FRAD is composed of a million micron-sized through-holes of a fluorinated polymer sheet cast on a coverslip glass (Figure 1a). For solution injection, the flow cell structure was constructed by assembling the fabricated device, a spacer sheet, and a top coverslip glass with an access port for injection of the solution. After the aqueous solution was introduced, the excess amount of solution was flushed with oil containing 10 mg/mL of 1,2-dioleoyl-*sn*-glycero-3-phosphocholine (DOPC) to stabilize the water−oil interface of the droplets. As a result, a million regularly shaped micron-sized droplets were displayed on the device. To facilitate the release of droplets from the FRAD, the glass surface at the bottom of the reactors was modified with polyethylene glycol (PEG). Owing to the high wettability of the PEG-modified surface,[45] the droplets spontaneously released from the side wall of the reactors while still attached on the PEG-modified glass surface (Figure 1b, Supplementary Movie 1). By gently tapping the flow cell or the microscope stage with a finger (Supplementary Movie 2),

https://dx.doi.org/10.1021/acsnano.0c04354
ACS Nano 2020, 14, 11700−11711

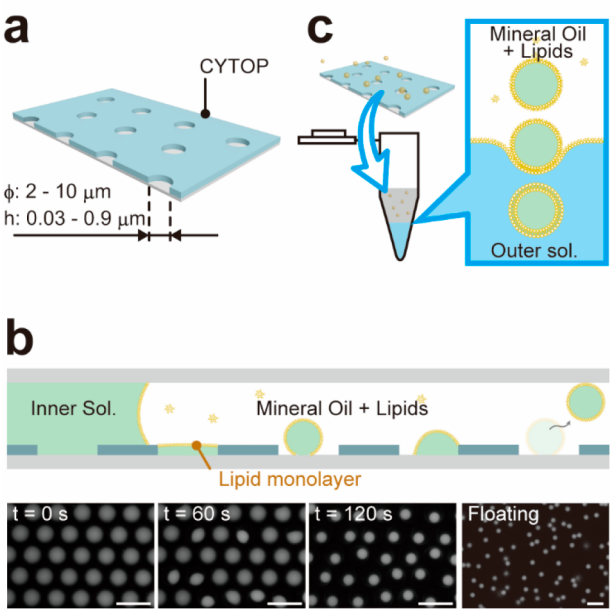

Figure 1. Production of uniform femto-liposomes. (a) Schematic image of the fabricated device containing more than 1000000 arrayed chambers (diameter: 2.2−9.8 μm; height: 26−910 nm). (b) Schematic (top) and fluorescence (bottom) images of the process for monodisperse emulsion droplet production. Aqueous solution was stained with Alexa Fluor 647 (10 μM) fluorescent dye in basal flow cell buffer, basal FCB (1 mM potassium phosphate at pH 7.5, 100 mM KCl, 2 mM $MgCl_2$, 500 mM sucrose). Excess solution was flushed with basal flow cell lipid, basal FCL (10 mg/mL DOPC in a mixture of 80% mineral oil and 20% chloroform). The detailed information on chemical compositions is provided in Supplementary Table S1. The inside chamber surface was modified with PEG2000. The formation of droplets was completed within 5 min. Scale bar, 10 μm. (c) Schematic image of the emulsion transfer method. Droplets were put in emulsion transfer lipid oil, ETL (2 mg/mL DOPG, 0.1 mg/mL cholesterol in 80% mineral oil and 20% chloroform mixture), placed on emulsion transfer buffer, ETB (1 mM potassium phosphate at pH 7.5, 100 mM KCl, 500 mM glucose, 5% (w/v) Pluoronic-F68), and then centrifuged. Liposomes were collected from the bottom of a centrifuge tube.

the droplets were readily released and became buoyant in the upper oil phase. The droplet release by tapping was highly efficient: 99.7% of the droplets were released in each preparation (Supplementary Figure S1). The release droplets were recovered from a flow chamber by manual pipetting. During this process, the significant fraction of droplets was lost (Figure S1a). Although this process remained to be optimized, for example, by use of micropump systems, the total number of droplets was still enough for the subsequent emulsion transfer process.

One may consider employing sonication treatment for droplet release rather than manual tapping of flow chamber device. However, sonication treatment was not efficient for droplet release and it also caused polydispersity of droplets due to random fusion among droplets. The droplet formation and release were repeatable over five times using a single device (Figure S2). The PEGylated device was stable for 3 weeks while the droplet generation efficiency slightly decreased after 4 weeks (Figure S1b), which would be improved after optimization of chemicals and device surface treatment.

The diameter of the released droplets was considered to be defined by the volume of the microreactors. To confirm this, various microreactors with different diameters and depths were tested. Figure 2a shows fluorescence images of the droplets with different diameters. The size distributions shown in Figure 2b obeyed a simple Gaussian distribution, with a small coefficient of variation (only 4−10%, regardless of droplet size). As a result, the diameter of the released droplets was consistent with that expected from the volume of the microreactors (Figure 2c).

Formation of Uniform Femto-liposomes. Liposomalization of w/o droplets was carried out by the bulk emulsion transfer method.[46] The droplet suspension was loaded onto the oil medium in a test tube holding the oil phase on the top and the water phase at the bottom, as illustrated in Figure 1c. The tube was centrifuged to spin down the droplets into the water phase. When the droplets passed through the oil−water interface, they were covered with the outer lipid layer to form liposomes. The production efficiency of liposomes from droplets is dependent on the centrifugal force and surface tension at the oil−water interface. The phase transfer yield decreased for smaller liposomes, as reported previously[47] (Figure S3). We found that the surfactant Pluronic F-68 reduces the surface tension to facilitate the emulsion transfer. We also tested several types of lipids and found that 1,2-dioleoyl-*sn*-glycero-3-phosphoglycerol (DOPG) provided the highest yield of liposome production (25%) (Figure S4). To gain higher gravitational forces for efficient emulsion transfer, we introduced sucrose inside the liposomes, while glucose was added to the external buffer medium at a concentration equivalent to that of sucrose for balancing the osmotic pressure. The sucrose/glucose concentration was changed from 50 to 500 mM. The lowest coefficient of variation of liposomes was obtained at 500 mM (Figure S5). Representative fluorescence images of liposomes prepared from droplets with various sizes are shown in Figure 3a. Figure 3b shows the size distributions. The variations were mostly comparable to those of droplets: the coefficient of variation was only 5−15%. The correlation between the diameter of the droplets and liposomes was very high, as seen in Figure 3c, showing that the diameter and volume of the liposomes are defined by the original volume of the microreactor on the FRAD.

Lamellarity of Liposomes. The unilamellarity of liposomes is indispensable for biological assays of membrane proteins such as membrane transporter proteins. To investigate the lamellarity of uniform femto-liposomes, we conducted transport assays of α-hemolysin, a transmembrane pore-forming toxin (ϕ = 1.5 nm) widely used as a model transporter protein owing to its ease in handling and measurement. Biotin-modified liposomes (ϕ = 2 μm) were prepared and tethered on the streptavidin-coated glass surface. For the detection of the transporting activity of α-hemolysin, the fluorescent dye Alexa Fluor 488 was encapsulated in the liposomes at 10 μM as the transport substrate (Figure 4a). When α-hemolysin was introduced at 100 μg/mL into the flow chambers, over 85% of liposomes exhibited the clear decay of fluorescent intensity (Figure 4b,c). The control experiments without α-hemolysin maintained the original fluorescent signal over time (gray line in Figure 4d). Thus, it was confirmed that 85% of the liposomes have a functional unilamellar lipid bilayer (Figure 4e). A possible reason for the 15% of nonreactive liposomes is that some liposomes have thicker bilayer containing emulsion transfer oil (see also the Conclusion for further discussion).

Digital Bioassay of α-Hemolysin. We then tested the feasibility of digital assay for α-hemolysin by limiting its

https://dx.doi.org/10.1021/acsnano.0c04354
ACS Nano 2020, 14, 11700−11711

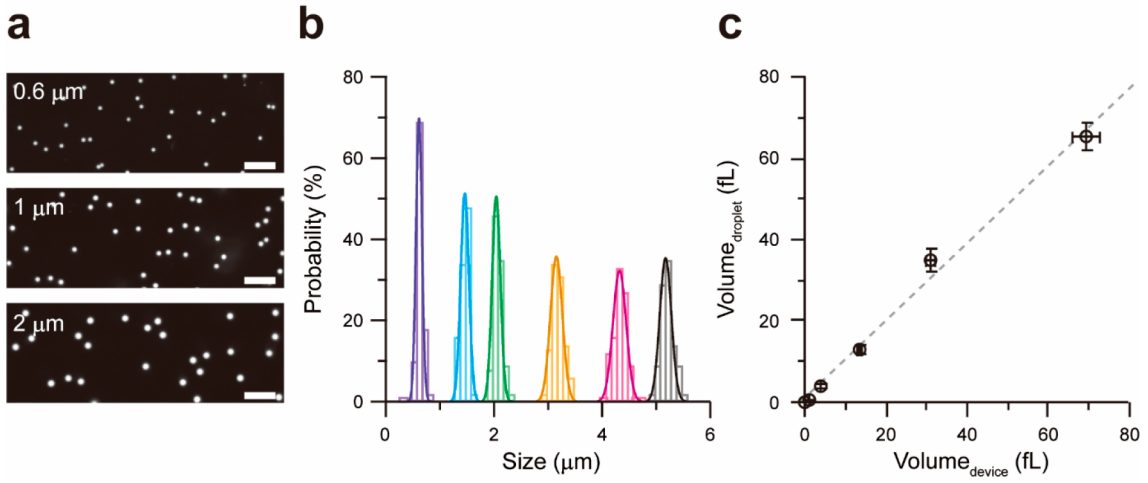

Figure 2. Size range and distribution of monodisperse emulsion droplets. (a) Representative fluorescence images of monodisperse droplets with different diameters. Scale bar, 10 μm. (b) Size distribution of droplets. Each droplet size was produced using microdevices with different volumes (Table S2). The solid lines are the Gaussian fitting for individual histograms, whose averages and corresponding deviations are 0.61 ± 0.08, 1.5 ± 0.1, 2.0 ± 0.1, 3.2 ± 0.2, 4.3 ± 0.2, and 5.2 ± 0.2 μm (from left to right). All histograms were calculated from at least 100 droplets. (c) Correlation between chamber volume and produced droplet volume. Error bars show the standard deviations. The gray dashed line is the linear fitting with a correlation coefficient of 0.98.

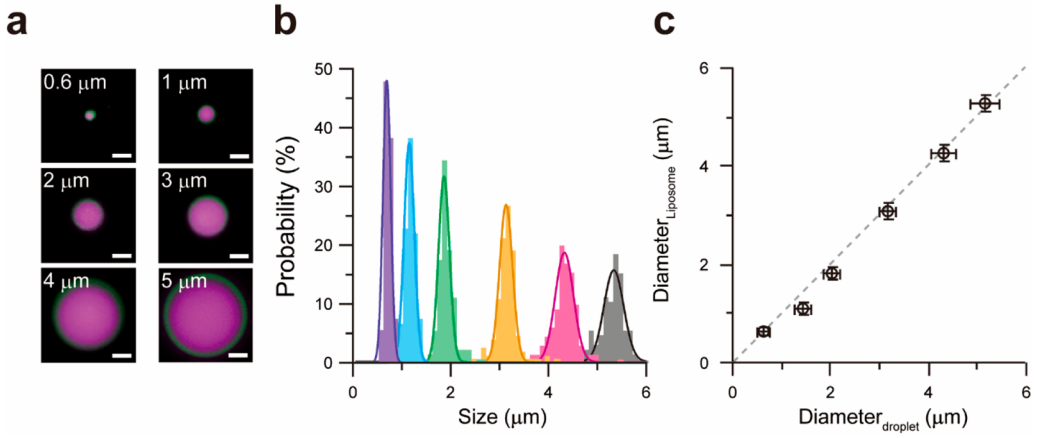

Figure 3. Size range and distribution of monodisperse liposomes. (a) Representative fluorescence images of monodisperse liposomes with various diameters. Liposome lumen and bilayer was fluorescently imaged with 10 μM Alexa Fluor 647 (magenta) or 0.01 mg/mL β-BODIPY 500/510 C_{12} (green). Detailed information on chemical composition is provided in Table S1. Scale bar, 1 μm. (b) Size distribution of liposomes. Each size of the liposomes was acquired from different droplet sizes. The solid lines are the Gaussian fitting for individual histograms, whose averages and corresponding deviations are 0.6 ± 0.1, 1.1 ± 0.1, 1.8 ± 0.2, 3.1 ± 0.2, 4.3 ± 0.2, and 5.3 ± 0.3 μm. All histograms were calculated from more than 100 liposomes obtained from three independent preparations. (c) Correlation between diameter of droplet and diameter of liposome. The error bars show the standard deviations. The gray dashed line is the linear fitting with a correlation coefficient of 1.0.

concentration. While α-hemolysin is soluble in aqueous solution as a monomer protein, it assembles into a homoheptamer ring on lipid membranes, forming a nanopore, herein referred to as an α-hemolysin nanopore molecule to facilitate passive transport of small chemicals. Thus, by introducing α-hemolysin solution to liposomes from outside, single molecules of α-hemolysin nanopores are stochastically formed on individual liposomes. α-hemolysin solution was introduced in the flow cell, on which 2 μm femto-liposomes were immobilized (Figure 4a), at a concentration of 0.1 μg/mL, according to our previous single-molecule measurements of α-hemolysin nanopore with the arrayed lipid bilayer chamber.[28,44] As expected, the liposomes showed the two distinctive activities (Figure 4b–f): 4% of the liposomes showed transport activity by exponentially decreasing the fluorescence signal, while the remaining 96% did not show a significant change. Figure 4d presents the typical time-courses of active liposomes that show a single exponential decay of fluorescence signal. The histogram of rate constants determined from the fluorescence decay showed distinct peaks (Figure 4g). Besides the leftmost peak, which corresponds to empty (nonactive) liposomes, there are one or two additional peaks. The second and third left peaks were attributed to the transporting activities of one or two molecules of α-hemolysin nanopores, respectively, for the following reasons. First, the rate constant was quantized, as seen in the distinct peaks in the histogram of the rate constants. Second, the intervals between the peaks, intervals of first-second and second-third peaks, are coincident. Third, the peak positions were not changed, irrespective of the concentration of α-

https://dx.doi.org/10.1021/acsnano.0c04354
ACS Nano 2020, 14, 11700–11711

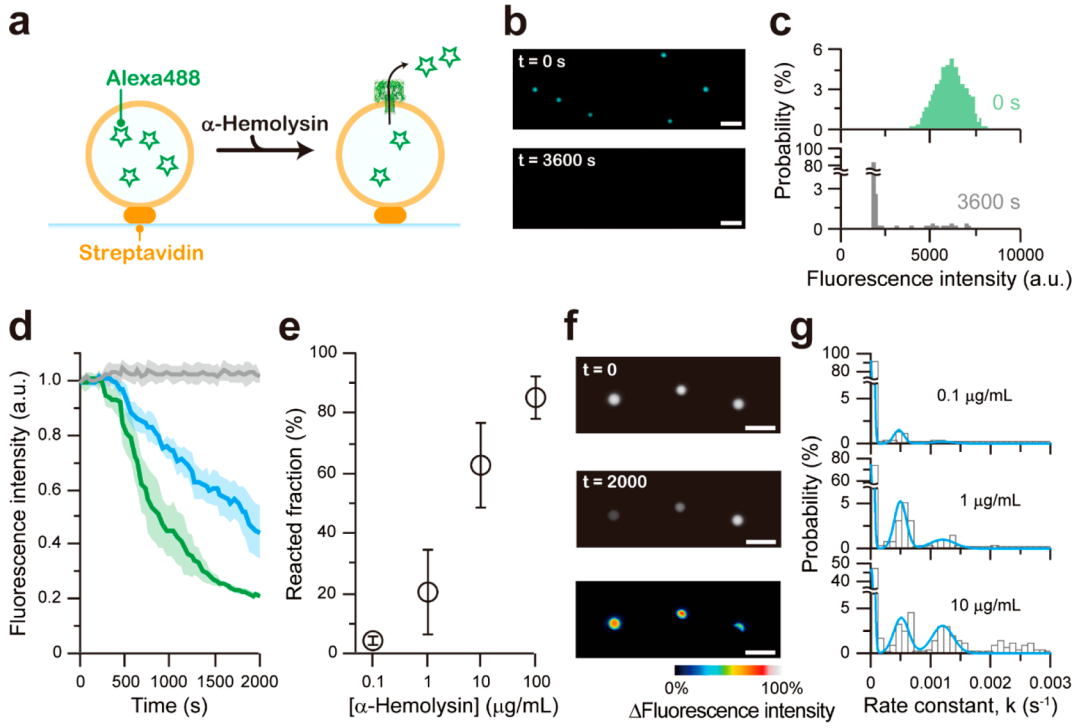

Figure 4. Fluorescence detection of passive transport *via* α-hemolysin. (a) Schematic image of passive transport by α-hemolysin nanopore. Alexa Fluor 488 (10 μM) was encapsulated in 2 μm liposomes as a transport substrate. Liposomes were prepared with 6 μg/mg biotin lipid and immobilized on a streptavidin-casted glass surface. Detailed information on chemical composition is provided in Table S1. (b) Fluorescence images of liposomes. The images were recorded at 0 and 3600 s after injection of 100 μg/mL α-hemolysin solution. Scale bar, 10 μm. (c) Histograms of fluorescence intensity of liposomes at 0 and 3600 s after injection of 100 μg/mL α-hemolysin. (d) Time-course of passive transport with 1 μg/mL α-hemolysin. Dark-colored lines represent the average fluorescence intensity of liposomes with zero (gray), one (blue), or two (green) molecules of α-hemolysin nanopore, estimated from the histogram analysis presented in (g). Light-colored shades show the standard deviations for each time point. (e) Concentration dependency of the fraction of reacted liposomes. Error bars show the standard deviations. (f) Fluorescence images of the passive transport of α-hemolysin observed in the single-molecule condition (0.1 μg/mL). The images were recorded immediately after the injection of α-hemolysin solution (0 s, top) and 2000 s later (middle). The bottom image is the differential image showing fluorescence change (color bar) between 0 and 2000 s. Scale bar, 5 μm. (g) Histogram of decay rate constants for passive transport. Decay rate constants were obtained from a single exponential fitting in (d). The width of bins is 10^{-4} s, and the solid lines are the Gaussian fitting. The passive transport activities of single molecules of α-hemolysin pore are 4.0 × 10^{-4}, 5.0 × 10^{-4}, and 4.0 × 10^{-4} s^{-1} at 0.1, 1, and 10 μg/mL, respectively.

hemolysin, while the area (*i.e.*, the number of liposomes) of each peak changed depending on the concentration of α-hemolysin. Fourth, the total number of active liposomes was proportional to the concentration of α-hemolysin (Figure 4e). These are typical features of single-molecule digital bioassays where the signal was quantized mostly into 0 and 1 due to the discreteness of the number of molecules, allowing for the quantification of biomolecules by counting the number of reactors showing positive signal.[1] The rate constant of the second left peaks, which corresponds to the activity of a single molecule of α-hemolysin nanopore, was determined to be (4–5) × 10^{-4}/s. This rate of fluorescence decay corresponds to the transport rate of approximately 10 molecules/s, which is consistent with our previous single-molecule analysis of α-hemolysin nanopore[28,44] conducted under the same concentration gradient of the substrate across the membranes.

Digital Bioassay of F_oF_1-ATPase. We then examined the feasibility of the digital assay of an active transporter protein with uniform femto-liposomes, considering their physiological and medical importance and the high demand for quantitative analysis of active transporter proteins.[27] In general, the quantitative measurement of active transporter proteins is challenging owing to their large and complex architectures with multisubunit compositions and lower transport activity, which are often coupled with large conformational changes. Because of these difficulties, most studies on uniform liposome preparation do not test the availability of active transport proteins. We measured the active H^+ pumping activity of F_oF_1-ATPase (F_oF_1) as a model active transporter protein by reconstituting it into uniform femto-liposomes. F_oF_1 interconverts proton motive force (*pmf*) across a membrane and free-energy of ATP *via* a rotary catalysis mechanism:[48] F_oF_1 actively pumps protons hydrolyzing ATP under low *pmf* conditions, while sufficient *pmf* drives F_oF_1 in the reverse direction, and ATP synthesis is coupled with H^+ translocation along the *pmf*. Detergent-solubilized F_oF_1 was directly incorporated into liposomes by suspending the precipitant of liposomes in the solution containing detergent-solubilized F_oF_1. The reconstituted F_oF_1 molecules expose F_1 outwardly due to the large water-soluble domain of F_1. F_oF_1 possesses catalytic sites for ATP hydrolysis on the water-soluble domain, thereby actively pumping H^+ from the outside into the inside of liposomes to acidify the inner medium of the liposomes (Figure 5a). Reconstituted liposomes were immobilized on the coverslip of a flow cell and observed under a fluorescence microscope. The reaction was initiated by the addition of ATP into a flow cell chamber. H^+ pumping activity was measured with a pH-sensitive fluorescent dye (RhP-M) that enhances

https://dx.doi.org/10.1021/acsnano.0c04354
ACS Nano 2020, 14, 11700–11711

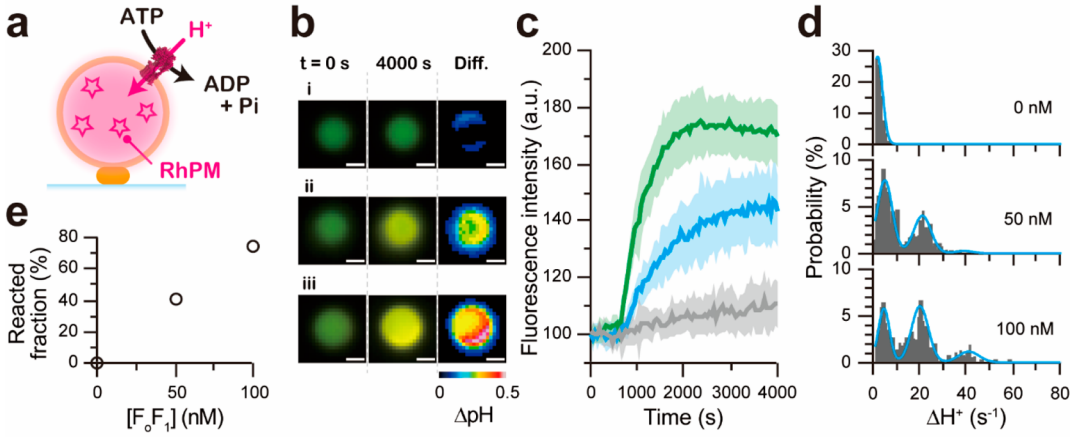

Figure 5. Single-molecule analysis of proton pumping by F_oF_1-ATPase. (a) Schematic image of proton pumping of F_oF_1-ATPase. To monitor in-liposome acidification upon proton pumping, 2 μm liposomes were prepared that contained a fluorescent pH indicator (20 μM RhP-M) in a low capacity buffer (0.1 mM HEPES pH 7.0). Detailed information on chemical composition is provided in Table S1. The F_oF_1-reconstituted liposomes were biotinylated and immobilized on the glass surface by biotin/streptavidin interaction as same as in the α-hemolysin experiment. (b) Fluorescence images of F_oF_1-reconstituted (100 nM) liposomes recorded with zero (i), one (ii), or two (iii) molecules of F_oF_1, estimated from the histogram analysis presented in (d). The right images are differential images showing pH change (color bar) between each image at 0 and 4000 s after injection of ATP. Scale bar, 1 μm. (c) Time-course of proton pumping. Deep-colored lines represent average fluorescence intensity of F_oF_1-reconstituted (100 nM) liposomes with zero (gray), one (blue), or two (green) molecules of F_oF_1, estimated from the histogram analysis presented in (d). Each time-course was obtained from more than 10 liposomes. The shades show the standard deviations. ATP was injected at 600 s. (d) Histogram of the proton pumping rate. The initial rate of proton pumping was determined from the initial 500 s by linear fitting. The bin size is 1 s^{-1}. The blue lines represent the Gaussian fittings. The proton pumping activities of single F_oF_1-ATPase are 18.6 and 19.1 s^{-1} at 50 and 100 nM F_oF_1 condition, respectively. The data in histograms were obtained from three independent preparations. (e) Concentration dependency of the fraction of reacted liposomes.

fluorescence upon acidification.[49] Unlike the digital assay with arrayed lipid bilayer chamber (ALBiC) device, nonspecific binding of pH probe dyes was not observed (Figure 5b), showing the superiority of these liposomes. When F_oF_1 was reconstituted at 100 nM, some liposomes showed a distinct increment of fluorescence signals, while others showed no obvious change in the signal (Figure 5b), suggesting stochastic reconstitution of the F_oF_1 molecule at the single-molecule level. The representative time-courses of fluorescence signals from positive liposomes (Figure 5c) show simple saturating curves of fluorescence signal. Active liposomes reached a plateau of fluorescence intensity at approximately 180, corresponding to pH 6.5. To confirm that their signal represents the proton pumping of F_oF_1, nigericin, an H^+ ionophore, was injected into the buffer to diminish the *pmf*. All active liposomes recovered the original fluorescence signal upon nigericin injection, confirming that the fluorescence increment represents active H^+ pumping.

The histogram of H^+-transporting activity that was determined from the initial rate in the time-courses exhibited distinct peaks (Figure 5d). The intervals between the peaks were almost constant, irrespective of the concentrations of F_oF_1 for reconstitution. These indicate that each peak represents the activity of 0, 1, or 2 molecules of F_oF_1. In addition, the observed λ, the mean number of F_oF_1 molecules per liposome, was well proportional to the amount of F_oF_1 injected for reconstitution (Figure 5e). Thus, the four criteria were satisfied and were in line with the results of the single-molecule transport assay for α-hemolysin, confirming that the second leftmost peak at nearly 20 H^+/s corresponds to the H^+-transporting activity of single-molecule F_oF_1. The rate of H^+-transport decreased with time, reaching a plateau level. This is reasonable because upon H^+-transport, the *pmf* is gradually formed, resulting in the suppression of the H^+-transport activity of F_oF_1. The plateau level for the single F_oF_1 molecule corresponds to pH 6.5; the resultant ΔpH (= $pH_{out} - pH_{in}$) is 0.5. At the same time, membrane voltage should be formed. Considering the buffering capacity of the inner core of liposomes, the number of transported protons is estimated to be nearly 30000 protons, which should generate a diffusion potential across the membrane at approximately 50 mV. In total, the generated *pmf* is estimated to be ca. 80 mV, which is sufficient to largely suppress the H^+-transporting activity of F_oF_1, although 80 mV is still below the thermodynamic equilibrium potential (around 200 mV).[50]

Digital Gene Expression. Finally, to demonstrate the versatility and biocompatibility of the uniform femto-liposomes for more complex biochemical reactions, we tested the feasibility of digital gene expression in uniform femto-liposomes by introducing the cell-free gene expression (*in vitro* translation and transcription, IVTT) system reconstituted from purified components (PURE system). First, we tested several types of lipids for flow cell lipid (FCL) that defines the lipid composition of the inner leaflet of bilayer. This is because the lipid composition can affect IVTT activity and protein activity.[51] Liposomes prepared with DOPC in FCL did not show detectable IVTT activity in consistent with the previous report.[51] 1,2-Dioleoyl-*sn*-glycero-3-phosphoethanolamine (DOPE) was not suitable for ETM process. The liposomes prepared from the mixture of 5 mg/mL of DOPC and 5 mg/mL of DOPE in FCL was found to ensure IVTT activity under the present conditions. The PURE system and plasmid DNA encoding β-galactosidase (β-gal) were encapsulated in the DOPC/DOPE liposomes. To compensate for the possible leakage of small chemicals from liposomes, the external medium contained molecules with low molecular weights for the PURE system, such as amino acids and nucleotides (for details, see the Methods).[52] The gene expression of β-gal was

https://dx.doi.org/10.1021/acsnano.0c04354
ACS Nano 2020, 14, 11700−11711

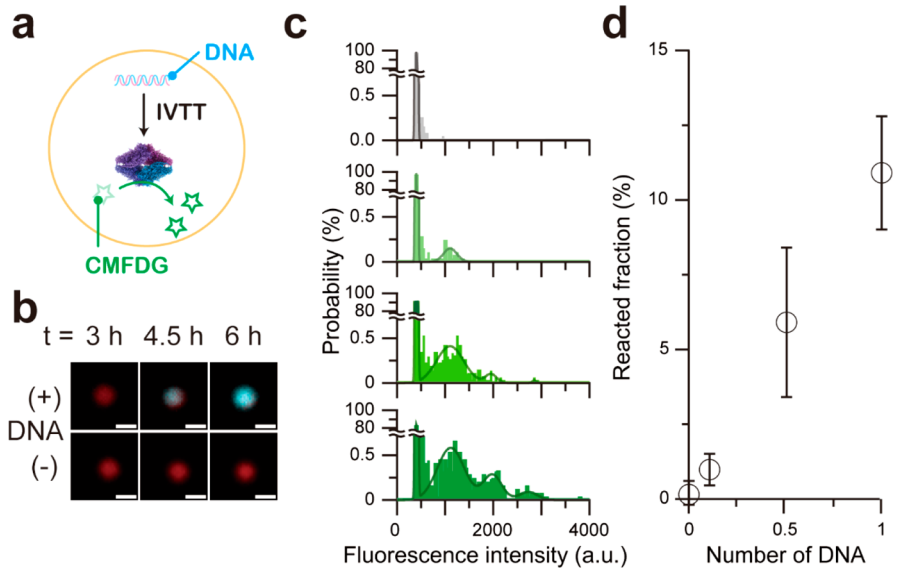

Figure 6. Cell-free gene expression in liposomes. (a) Schematic image of cell-free gene expression of β-gal. IVTT systems, DNA encoding β-gal, and fluorogenic substrate (CMFDG) were encapsulated in the liposomes prepared with 5 mg/mL of DOPC and 5 mg/mL of DOPE as the inner leaflet lipid composition to ensure IVTT activity. Detailed information on chemical composition is provided in Table S1. β-Gal expressed using the IVTT system cleaved the fluorogenic substrate, resulting in the increase of fluorescence intensity of the product (CMF). (b) Fluorescence image of expression/catalysis of β-gals in the presence (upper)/absence (bottom) of DNA. The images were recorded at t = 3 h (left), 4.5 h (middle), 6 h (right). The liposome was visualized by the encapsulation of Alexa Fluor 647 (red). The fluorescence of CMF was shown by cyan. Scale bar, 2 μm. (c) Histogram of fluorescence intensity of CMF. The bin is 50 au, and the solid lines represent the Gaussian fitting. DNA solution was encapsulated in liposomes at 0, 45, 225, and 450 nM that corresponds to the mean number of DNA molecules per liposome (λ) of 0, 0.1, 0.5, and 1, respectively. (d) Correlation between the fraction of reacted liposomes and the number of encapsulated DNA. Error bars show the standard deviations.

detected with a fluorogenic assay where β-gal enzymes cleave the fluorogenic substrate 5-chloromethylfluorescein di-β-D-galactopyranoside (CMFDG) to produce fluorescent 5-chloromethylfluorescein (CMF) (Figure 6a). After an incubation period of over 3 h at room temperature, the fluorescence signal appeared in DNA (+) liposomes showing the active gene expression of β-gal enzymes, whereas DNA (−) liposomes did not show fluorescence signals (Figure 6b). Figure 6c shows the distribution of fluorescence intensity after incubation for 12−15 h. As seen in the above-mentioned single-molecule digital assays, the fluorescence signal of liposomes expressing β-gal was also quantized. The four features of the single-molecule digital bioassay were again observed in the cell-free gene expression: signal quantization, constant intervals between peaks, concentration-independent activity for each peak, and concentration-dependent population of active reactors. Thus, digital gene expression in uniform femto-liposomes was confirmed. It should be noted that the observed λ (the mean number of DNA molecules per liposome) was always 10 times lower than the value expected from the initially introduced DNA concentration (Figure 6d). The exact reason is unknown, but it is attributable to the loss of DNA molecules prior to encapsulation in liposomes by nonspecific absorption of DNA on the surface of the test tube or FRAD device. This remains to be resolved.

CONCLUSION

We established a simple method for the preparation of monodisperse and bacterial cell-sized liposomes, termed uniform femto-liposomes, with the aim to establish digital bioassays for membrane proteins and complex biosystems. This was achieved by combining FRAD and the optimized emulsion transfer method. The developed protocol has several key features for the reproducible production of uniform femto-liposomes. First, we established the protocol for femto-droplet generation, in which >1000000 homogeneous droplets displayed on the FRAD are released into the oil medium simultaneously. The wettability of the PEG-modified reactor surface enables the highly efficient droplet preparation,[45] while FRAD without PEG modification shows low efficiency. The second key improvement is the optimization of the emulsion transfer method (ETM) for efficient production of micron-sized liposomes, which is difficult in conventional ETM. The addition of surfactant into the aqueous phase decreases the surface tension at the oil−water interface, facilitating the production of femto-liposomes. Accordingly, the choice of the lipid molecules and the concentration of sucrose and glucose were also important for optimization of the protocol. Consequently, these improvements allowed the production of uniform femto-liposomes, from 0.6 to 5.3 μm, with high monodispersity (coefficient of variation: 5−15%). Since the droplets were rarely fused or divided during the preparation, it was confirmed that the size of droplets and liposomes is defined by the volume of the microreactor. This protocol took approximately 1 h for all processes. Approximately 180000 liposomes were produced from a single microdevice, that is, the throughput for liposome production is 180000 liposomes/h (~50 liposomes/s). This throughput is equivalent to the ones using microfluidics (tens of hertz).[38] The use of a greater number of droplets by parallel processing with multiple devices or repeated production of droplets would increase the total production of uniform femto-liposomes by a factor of 5−10.

We should also note some restrictions and technical challenges of this method. From the principle of ETM, the inside solution of femto-liposome has to contain sucrose at

https://dx.doi.org/10.1021/acsnano.0c04354
ACS Nano 2020, 14, 11700−11711

hundreds mM level or other additives to gain higher density. Some protein or macromolecule-crowded solutions might not be suitable as the in-liposome solution, considering that nondiluted *in vitro* translation and translation (IVTT) solution stuck to FRAD device and was not released from the device unless diluted to 70%. Within restrictions, various types of biologically relevant solutions would be available for this method. In addition, this method has clear preference for lipid composition (Figure S4). Another restriction of this protocol is the requirement of surfactant to reduce surface tension at the oil−water interface for efficient ETM. Among the surfactants tested, Pluronic F-68 is the best to produce uniform femto-liposomes. Although decyl maltoside was also found to be suitable for ETM, it also caused lipid aggregates, hampering reconstitution and the subsequent assay of membrane proteins.

A remaining technical challenge is the heterogeneous quality of the liposomes found in the α-hemolysin assay: 15% of the liposomes did not show the passive transporting activity in the presence of excess amounts of α-hemolysin. This suggests that a fraction of uniform femto-liposomes is not available to support the functionality of membrane proteins. One possible explanation is the presence of multilamellar liposomes. According to previous reports on ETM, however, more than 95% of the ETM-produced liposomes have a unilamellar membrane.[46,47] Another possibility is that the remnant oil, which thickens the lipid bilayer more than biological membranes, hampers the functionality of membrane proteins. This is a common drawback of ETMs and other liposome preparation methods that use nonvolatile oils. Oil-free methods for uniform liposome preparation are warranted to circumvent this problem.

The uniform femto-liposomes enabled the quantitative digital bioassays for membrane proteins. The monodispersity of liposomes is one of the critical factors for the quantitative analysis of transporting activity. Most measurements of transporting activity use fluorescent indicator dyes encapsulated in liposomes. Assays performed on polydisperse liposomes principally display heterogeneous response of indicators. The size of liposomes is also another critical factor. When the size is too large, the signal changes of the indicator dyes should be correspondingly slow for the detection. Meanwhile, when the size of the liposomes is too small, the signal changes should be too fast and too small. Thus, depending on the rate of transporting activity and the nature of the indicator dyes, the size of liposomes must be adjusted to a right size. To show the feasibility of our liposomes, we demonstrated digital bioassays of transporter assays: passive transport measurements of single molecules of α-hemolysin nanopore and active transport measurements of F_oF_1 ATP synthase. We determined the transporting activities as 10 turnover/s for α-hemolysin nanopore and 20 turnover/s for ATP synthase, which are consistent with previous data.[28]

We also demonstrated digital gene expression by encapsulating *in vitro* a transcription−translation mixture with single DNA molecules. The micron-sized uniform femto-liposomes would be suitable for future cell-free synthetic biology studies. This is because surface area-to-volume ratio of the femto-liposome coincide well with that of natural bacterial cells, 3−8 μm^{-1}.[53] In addition, it was reported that a protocell model liposome with an RNA replicator system showed the maximum RNA replication activity within micron-sized liposomes.[54] The uniform femto-liposome would enable quantitative analysis of designed gene circuits with a single set of DNA molecules that would uncover fundamental stochastic features masked in ensemble averaging.

Thus, the present study demonstrates that the uniform femto-liposomes are versatile for many applications, from single-molecule analysis of membrane proteins to cell-free synthetic biology studies. A remaining challenge is to implement the functionality for active morphological changes of liposomes, such as active fusion, fission, tubing, and division. This potential differentiates liposomes from other femto reactors embedded in microsystems or microdevices. In preliminary experiments, we observed morphological changes of uniform femto-liposomes upon osmotic pressure change (Figure S6). The reconstitution of membrane-associating proteins[55,56] or enzymes that synthesize lipid molecules[57] would endow morphological dynamics to uniform femto-liposomes.

MATERIALS AND METHODS

Preparation of the PEG-Coated Device. A femtoliter reactor array device (FRAD) was prepared as described previously[13,28] with the following modifications. Hydrophobic carbon−fluorine (CYTOP; AGC, Tokyo, Japan) polymer was spin-coated at 2000 or 4000 rpm for 30 s on a SiO_2 glass coverslip (32 × 24 mm^2, custom-ordered; Matsunami, Osaka, Japan) and baked at 90 °C for 10 min and then at 180 °C for 1 h to evaporate the solvent. A positive photoresist (AZP4903; AZ Electronic Materials, Japan) was spin-coated on the CYTOP layer at 7500 rpm for 30 s and then exposed to UV for 8 s for patterning the mask structure. For the preparation of chambers of different sizes, we used CYTOP at 1−9% (w/v) to change the depth of the reactors (Table S2). To expose the hydrophilic SiO_2 glass surface, the resist-patterned substrate was etched with O_2 plasma for 7 min. The pegylation of the bottom glass surface of the reactors was carried out as described in a previous study[58] with the following modifications. First, SH-silane was coated on an exposed SiO_2 glass surface and CYTOP surface inside the chambers by immersing the device in a silane solution (1% (v/v) SH-silane (KBM-803; Shinetsu, Japan), 0.1% (v/v) acetic acid in Milli-Q (Millipore) at 90 °C for 2 h. Next, the silane-coated substrate was baked at 110 °C for 10 min. Then the substrate was immersed into 0.1 M K-Pi (pH = 7.5) with 20 mg/mL mal-PEG2000 (ME-020MA; NOF, Japan) for 2 h at room temperature. The remaining photoresist was removed using acetone and rinsed with 2-propanol. Finally, the substrate was washed with Milli-Q water and dried under nitrogen flow. We were able to efficiently fabricate hydrophobic through-hole structures on a hydrophilic SiO_2 glass coverslip, with a fabrication success rate of ∼100%. The depth and height of the fabricated chambers were measured by 3D laser scanning confocal microscopy (VK-X210; KEYENCE, Japan) (Table S2).

Medium Composition for Droplet Preparation and Liposome Formation. The preparation of uniform femto-liposome is principally composed of two steps: *preparation of uniform droplet* and *emulsion transfer for liposome formation*. Each step uses an aqueous buffer medium and a lipid-in-oil medium. The buffer medium and the lipid medium in *preparation of uniform droplet* define the inner-liposome medium and the lipid composition of inner leaflet of liposome bilayer, respectively. These mediums are termed *flow cell buffer* (*FCB*) and *flow cell lipid* (*FCL*), considering that the droplets were prepared in a flow cell. The buffer solution and the lipid solution in *preparation of uniform droplet* by the use of emulsion transfer method define the external-liposome medium and the lipid composition of outer leaflet of liposome bilayer, respectively. Those are termed *emulsion transfer buffer* (*ETB*) and *emulsion transfer lipid* (*ETL*). The solution and lipid compositions are slightly/largely modified in each experiment. For clarification, the total list of solution and lipid compositions are provided in Table S1. The below is the basal protocols for droplet formation and liposome formation.

Preparation of Uniform Droplet. The flow cell was constructed by assembling a fabricated device, a 0.2 mm-thick spacer sheet (SLF-

https://dx.doi.org/10.1021/acsnano.0c04354
ACS Nano 2020, 14, 11700−11711

0601; Bio-Rad, Japan), and a CYTOP-coated glass block with an access port for solution injection. The flow cell was filled with flow-cell buffer (FCB). The basal composition of FCB is 1 mM potassium phosphate, 100 mM KCl, 500 mM sucrose. For fluorescence imaging, 10 μM Alexa Fluor 488 or Alexa Fluor 647 (A10254 or A20347; Thermo Fisher Scientific, USA) was added in FCB (Table S1). Then, FCB in a flow cell was flushed out by flow cell lipid (FCL). The basal FCL composition is 10 mg/mL DOPC (MC-8181; NOF, Japan) dissolved in a mixture of chloroform and mineral oil (2:8 (v/v)). After spontaneous formation of droplets on the FRAD reactors, the device was tapped gently to release the droplets from the reactors. The processes of droplet formation and release were recorded in Supplementary Movies 1 and 2. The released droplets in FCL were collected by pipetting.

Emulsion Transfer for Liposome Formation. Liposomes were prepared using emulsion transfer method,[47,59] with modifications. The basal emulsion transfer lipid (ETL) solution (2 mg/mL DOPG and 0.1 mg/mL cholesterol) was prepared as follows: 20 μL of 100 mg/mL DOPG (MG-8181LS; NOF) and 1 μL of 100 mg/mL cholesterol (034-03002; Wako, Japan), each predissolved in chloroform, were mixed into 980 μL of mineral oil (M-5904; Sigma-Aldrich, Japan). Chloroform in the lipid mixture was then evaporated in the incubation at 80 °C for 20 min with a dry block bath. When indicated, a fluorescent lipid (β-BODIPY 500/510 C_{12}−HPC DHCP, D3793; Thermo Fisher Scientific, USA) and/or a biotinylated lipid (B1616; Thermo Fisher Scientific, USA) dissolved in chloroform was spiked into ETL before chloroform evaporation at the final concentration of 10 μg/mL and 0.006 mg/mL, respectively. ETL (400 μL) was mixed with 20 μL of droplets in FCL and then layered on 400 μL of emulsion transfer buffer (ETB) in a 1.5 mL test tube. ETB is composed of basal ETB (1 mM potassium phosphate, 100 mM KCl, and 500 mM glucose; pH adjusted to 7.5) and 5% (w/v) Pluoronic-F68 (24040032; Thermo Fisher Scientific). After the layered ETL and ETB in a test tube were left to stand for 20 min at 25 °C, the test tube was centrifuged at 21900g for 30 min at 25 °C for emulsion transfer. After centrifugation, ETL and supernatant of ETB were gently removed by pipetting. The precipitated liposomes were suspended in 400 μL of ETB and collected. For lipid aggregate removal, the liposome suspension was recentrifuged at 21900g for 10 min at 25 °C, and the supernatant was gently removed. Finally, we obtained 40 μL of liposome dispersion.

Microscopy. Epi-fluorescence images of liposomes were taken with an inverted microscope Ti-E (Nikon, Japan) equipped with 100× and 60× objective lenses, a digital CMOS camera (ORCA-flash4.0; Hamamatsu Photonics, Japan), and an LED light source (Sola, Lumencor, USA) to provide illumination with filter sets (from Semrock, USA or Nikon, Japan): (i) excitation (Ex): 480/40 nm, dichroic: 505 nm, emission (Em): 535/50 nm for Alexa Fluor 488 and CMF; (ii) Ex: 554/23 nm, dichroic: 573 nm; Em: 609/54 nm for RhP-M; and (iii) Ex: 630/38 nm, dichroic: 655 nm, Em: 694/44 nm for Alexa Fluor 647. The microscope system was controlled by NIS elements (Nikon, Japan).

Image Analysis for Size Determination. A flow cell was assembled by placing two double-sided tapes (thickness: ∼0.1 mm) onto a coverslip (36 × 24 mm^2) with another coverslip (20 × 20 mm^2, Matsunami, Japan) on top. Immediately before use, liposome suspension was gently pipetted to obtain a homogeneous dispersion and then infused into the flow cell that was sealed with nail polish. Liposomes were settled down on the bottom coverslip owing to the higher specific density gravity of inner medium of liposomes and were observed for size analysis. We set the threshold at 40% of the peak intensity of encapsulated dye and defined the edge-to-edge distance of the fluorescence image as the diameter of the liposomes (Figure S7). The size of the droplets was determined in the same manner.

Passive Transport Analysis. Liposomes for the passive transport analysis of α-hemolysin were prepared by spiking, into the basal ETL, a biotinylated lipid at a final concentration of 0.006 mg/mL for stable immobilization on the bottom of a flow cell chamber. As a fluorescent substrate for transport activity of α-hemolysin, 10 μM Alexa Fluor 488 was added in FCB. The flow cell chamber was prepared by assembling a glass coverslip (thickness: 120−170 μm, Matsunami, Japan), a spacer sheet, and CYTOP-coated glass block with an access port for the injection of medium. A solution of 1 mg/mL streptavidin (PRO-791; ProSpec, Israel) in 1 mM potassium phosphate and 100 mM KCl (pH adjusted to 7.5) was introduced in a flow cell chamber and incubated for 20 min at room temperature for nonspecific streptavidin coating of the flow cell chamber. The unbound streptavidin was removed by flushing the flow chamber with the basal ETB. Liposomes with biotinylated lipids were introduced into the flow cell chamber. After incubation for 2 h, unbound liposomes were washed out with the basal ETB. Passive transport measurements were initiated by the injection of α-hemolysin (HP101; Toxin Technology, USA) at 0.1−100 μg/mL into the flow cell chamber. Fluorescence images were acquired at 40 s intervals. The analysis of passive transport was performed as described previously.[28,44] The detailed information on the mediums was provided in Table S1.

Preparation of F_oF_1. A mutated F_oF_1 from *Bacillus* PS3, herein referred to as F_oF_1 for simplicity, which has a 10-histidine tag at the N terminus of the β subunit and lacks the C terminal of the ϵ subunit, was used in this study.[60] F_oF_1 was expressed and purified as described previously[61] with the following modifications. F_oF_1 was solubilized in a solution (10 mM HEPES, 5 mM $MgCl_2$, 10% (v/v) glycerol, with the pH adjusted to 7.5 with KOH) containing 0.5% (w/v) LMNG (NG310; Anatrace, USA). Ni-sepharose resin was pre-equilibrated with the M buffer (20 mM K-Pi and 100 mM KCl, pH 7.5) containing 0.005% LMNG. After the binding of F_oF_1 to the resin, the resin was washed with M buffer containing 20 mM imidazole and 0.005% LMNG. F_oF_1 was eluted with M buffer containing 200 mM imidazole and 0.005% LMNG.

Analysis of Proton Pumping by F_oF_1. Liposomes with biotinylated lipids were prepared by spiking, into the basal *ETL*, a biotinylated lipid at the final concentration of 0.006 mg/mL. For the measurement of proton pumping activity by single-molecule of F_oF_1, we prepared the FCB medium with a low buffering capacity of 0.1 mM HEPES (Supporting Table S1), into which 20 μM RhP-M was added as the fluorescent pH indicator.[49] For the reconstitution of F_oF_1 into the liposomal membrane, F_oF_1 was added, at the indicated concentration, to the ETB medium for the F_oF_1 measurement (Supporting Table S1). The ETB medium with reconstituted liposomes was introduced into a flow cell chamber prepared as same as in the α-hemolysin experiment. After 2 h incubation, the unbound liposomes and F_oF_1's were washed out with the ETB medium. Proton pumping of F_oF_1 was initiated by the injection of ATP at 200 μM in the ETB medium. Fluorescence images were acquired at 50 s intervals. The rate of proton pumping activity was determined as described previously[28] with slight modifications as described in the Supporting Information.

Plasmid Preparation for Cell-Free Gene Expression. Cell-free gene expression of β-galactosidase was carried out using a reconstituted *in vitro* transcription-translation system (IVTT).[62] A DNA plasmid encoding β-galactosidase was prepared by ligation into the *Bam*HI and *Hind*III site in the vector using the pRSET vector (V35120; Thermo Fisher Scientific, USA). The constructed plasmid was transferred into *E. coli* JM109-competent cells (9052; Takara, Japan), which were cultured for amplification. The amplified DNA plasmid was purified using the NucleoSpin Plasmid QuickPure kit (740615; Takara, Japan). The concentration of the DNA plasmid was determined by measuring the absorbance at 260 nm.

Gene Expression in Liposome. The liposomes for *in vitro* transcription and translation (IVTT) were prepared along the protocol above-mentioned with several modifications. FCL medium contained 5 mg/mL DOPC and 5 mg/mL DOPE, and ETL medium contained a biotinylated lipid at the final concentration of 0.006 mg/mL. For encapsulation of IVTT components, FCB medium contained 70% diluted IVTT solution (PURExpress; NEB, USA) with plasmid DNA at the indicated concentration. ETB medium was largely different from the others; ETB contained small chemicals (amino acids, reducing reagents, and so on) in IVTT components (Table S1. This is to supply these chemicals that might leak from liposomes. The complete list of chemicals used in mediums was provided in Table S1.

https://dx.doi.org/10.1021/acsnano.0c04354
ACS Nano 2020, 14, 11700−11711

Before the droplet preparation, flow cell chambers were treated with a blocking solution (1 mM potassium phosphate, 100 mM KCl, 0.01% LMNG) in order to avoid nonspecific absorption of IVTT components to the inner surface of a flow cell chamber. The protocols for droplet formation, emulsion transfer for liposome formation, and liposome immobilization were as same as in the α-hemolysin and F_oF_1 measurements. Liposomes were incubated for 12−15 h in flow cell chambers before the recording of fluorescent image.

ASSOCIATED CONTENT

Supporting Information

The Supporting Information is available free of charge at https://pubs.acs.org/doi/10.1021/acsnano.0c04354.

Efficiencies at each step of the droplet formation procedure, size distribution of the droplets using a repeated microdevice, emulsion transfer method using polydisperse droplets, number of liposomes prepared with various lipids and surfactants, size distribution of liposomes prepared with chamber of 5 μm at different concentrations of sugar, osmotic pressure-driven morphological changes of liposomes, determination of liposome size, calibration curve of the fluorescence intensity of RhP-M (Figure S1−S8), chemical compositions of buffer, lipid solutions, fabrication protocols and size information for each chamber and resulting droplets and liposomes (Table S1 and S2), supplementary method for determination of proton pumping activity of F_oF_1, and supplementary references (PDF)

Real time movies of water-in-oil droplet deformation (Movie 1) (AVI)

Real time movie of droplet release from reactors (Movie 2) (AVI)

AUTHOR INFORMATION

Corresponding Author

Hiroyuki Noji − *Department of Applied Chemistry, Graduate School of Engineering, The University of Tokyo, Tokyo 113-8656, Japan;* orcid.org/0000-0002-8842-6836; Email: hnoji@appchem.t.u-tokyo.ac.jp

Authors

Naoki Soga − *Department of Applied Chemistry, Graduate School of Engineering, The University of Tokyo, Tokyo 113-8656, Japan*

Akira Ota − *Department of Applied Chemistry, Graduate School of Engineering, The University of Tokyo, Tokyo 113-8656, Japan*

Kota Nakajima − *Department of Applied Chemistry, Graduate School of Engineering, The University of Tokyo, Tokyo 113-8656, Japan*

Rikiya Watanabe − *Department of Applied Chemistry, Graduate School of Engineering, The University of Tokyo, Tokyo 113-8656, Japan; PRIME, Japan Agency for Medical Research and Development, Tokyo 100-0004, Japan*

Hiroshi Ueno − *Department of Applied Chemistry, Graduate School of Engineering, The University of Tokyo, Tokyo 113-8656, Japan;* orcid.org/0000-0001-5331-4335

Complete contact information is available at: https://pubs.acs.org/10.1021/acsnano.0c04354

Author Contributions

N.S., R.W., and N.H. designed the experiments; N.S., A.O., and K.N. performed the experiments and analyzed the data; N.S., H.U., and N.H. wrote the paper.

Notes

The authors declare no competing financial interest.

ACKNOWLEDGMENTS

This work was supported by Grant-in-Aid for Scientific Research on Innovative Area (JP17H05717) to N.S., Precursory Research for innovative Medical Care (PRIME) Grant from the Japan Agency for Medical Research and Development (JP17gm0910020) to R.W., ImPACT Program of Council for Science, Technology, and Innovation (Cabinet Office, Government of Japan) to H.N., Grant-in-Aid for Scientific Research (S) (JP19H05624) to H.N., and JST CREST, Japan (JPMJCR19S4) to H.N.. We thank H. Suzuki and M. Tsugane for technical advice on the emulsion transfer method, Y. Urano and M. Kamiya for kindly providing the fluorescent pH indicator, N. Ichihashi for technical advice on the protein expression experiments, the members of Noji Laboratory for discussion and advice, and K. Ota for the encouragement and laboratory management. The authors declare no competing interests.

REFERENCES

(1) Zhang, Y.; Noji, H. Digital Bioassays: Theory, Applications, and Perspectives. *Anal. Chem.* **2017**, *89*, 92−101.

(2) Walt, D. R. Protein Measurements in Microwells. *Lab Chip* **2014**, *14*, 3195−3200.

(3) Witters, D.; Sun, B.; Begolo, S.; Rodriguez-Manzano, J.; Robles, W.; Ismagilov, R. F. Digital Biology and Chemistry. *Lab Chip* **2014**, *14*, 3225−3232.

(4) Rissin, D. M.; Walt, D. R. Digital Concentration Readout of Single Enzyme Molecules Using Femtoliter Arrays and Poisson Statistics. *Nano Lett.* **2006**, *6*, 520−523.

(5) Rondelez, Y.; Tresset, G.; Tabata, K. V.; Arata, H.; Fujita, H.; Takeuchi, S.; Noji, H. Microfabricated Arrays of Femtoliter Chambers Allow Single Molecule Enzymology. *Nat. Biotechnol.* **2005**, *23*, 361−365.

(6) Baker, M. Digital PCR Hits Its Stride. *Nat. Methods* **2012**, *9*, 541−544.

(7) Tabata, K. V.; Minagawa, Y.; Kawaguchi, Y.; Ono, M.; Moriizumi, Y.; Yamayoshi, S.; Fujioka, Y.; Ohba, Y.; Kawaoka, Y.; Noji, H. Antibody-Free Digital Influenza Virus Counting Based on Neuraminidase Activity. *Sci. Rep.* **2019**, *9*, 1067.

(8) Vogelstein, B.; Kinzler, K. W. Digital PCR. *Proc. Natl. Acad. Sci. U. S. A.* **1999**, *96*, 9236−9241.

(9) Diehl, F.; Li, M.; He, Y.; Kinzler, K. W.; Vogelstein, B.; Dressman, D. BEAMing: Single-Molecule PCR on Microparticles in Water-in-Oil Emulsions. *Nat. Methods* **2006**, *3*, 551−559.

(10) Kim, S. H.; Iwai, S.; Araki, S.; Sakakihara, S.; Iino, R.; Noji, H. Large-Scale Femtoliter Droplet Array for Digital Counting of Single Biomolecules. *Lab Chip* **2012**, *12*, 4986−4991.

(11) Rissin, D. M.; Kan, C. W.; Campbell, T. G.; Howes, S. C.; Fournier, D. R.; Song, L.; Piech, T.; Patel, P. P.; Chang, L.; Rivnak, A. J.; Ferrell, E. P.; Randall, J. D.; Provuncher, G. K.; Walt, D. R.; Duffy, D. C. Single-Molecule Enzyme-Linked Immunosorbent Assay Detects Serum Proteins at Subfemtomolar Concentrations. *Nat. Biotechnol.* **2010**, *28*, 595−599.

(12) Rotman, B. Measurement of Activity of Single Molecules of β-D-Galactosidase. *Proc. Natl. Acad. Sci. U. S. A.* **1961**, *47*, 1981−1991.

(13) Sakakihara, S.; Araki, S.; Iino, R.; Noji, H. A Single-Molecule Enzymatic Assay in a Directly Accessible Femtoliter Droplet Array. *Lab Chip* **2010**, *10*, 3355−3362.

(14) Shen, F.; Davydova, E. K.; Du, W.; Kreutz, J. E.; Piepenburg, O.; Ismagilov, R. F. Digital Isothermal Quantification of Nucleic Acids *via* Simultaneous Chemical Initiation of Recombinase Polymerase Amplification Reactions on Slipchip. *Anal. Chem.* **2011**, *83*, 3533−3540.
(15) Kiss, M. M.; Ortoleva-Donnelly, L.; Beer, N. R.; Warner, J.; Bailey, C. G.; Colston, B. W.; Rothberg, J. M.; Link, D. R.; Leamon, J. H. High-Throughput Quantitative Polymerase Chain Reaction in Picoliter Droplets. *Anal. Chem.* **2008**, *80*, 8975−8981.
(16) Kumaresan, P.; Yang, C. J.; Cronier, S. A.; Blazej, R. G.; Mathies, R. A. High-Throughput Single Copy DNA Amplification and Cell Analysis in Engineered Nanoliter Droplets. *Anal. Chem.* **2008**, *80*, 3522−3529.
(17) Hatori, M. N.; Kim, S. C.; Abate, A. R. Particle-Templated Emulsification for Microfluidics-Free Digital Biology. *Anal. Chem.* **2018**, *90*, 9813−9820.
(18) Gansen, A.; Herrick, A. M.; Dimov, I. K.; Lee, L. P.; Chiu, D. T. Digital Lamp in a Sample Self-Digitization (SD) Chip. *Lab Chip* **2012**, *12*, 2247−2254.
(19) Zhu, Q.; Gao, Y.; Yu, B.; Ren, H.; Qiu, L.; Han, S.; Jin, W.; Jin, Q.; Mu, Y. Self-Priming Compartmentalization Digital Lamp for Point-of-Care. *Lab Chip* **2012**, *12*, 4755−4763.
(20) Wang, J.; Kreutz, J. E.; Thompson, A. M.; Qin, Y.; Sheen, A. M.; Wang, J.; Wu, L.; Xu, S.; Chang, M.; Raugi, D. N.; Smith, R. A.; Gottlieb, G. S.; Chiu, D. T. SD-Chip Enabled Quantitative Detection of HIV RNA Using Digital Nucleic Acid Sequence-Based Amplification (dNASBA). *Lab Chip* **2018**, *18*, 3501−3506.
(21) Obayashi, Y.; Iino, R.; Noji, H. A Single-Molecule Digital Enzyme Assay Using Alkaline Phosphatase with a Cumarin-Based Fluorogenic Substrate. *Analyst* **2015**, *140*, 5065−5073.
(22) Ehrl, B. N.; Liebherr, R. B.; Gorris, H. H. Single Molecule Kinetics of Horseradish Peroxidase Exposed in Large Arrays of Femtoliter-Sized Fused Silica Chambers. *Analyst* **2013**, *138*, 4260−4265.
(23) Liebherr, R. B.; Renner, M.; Gorris, H. H. A Single Molecule Perspective on the Functional Diversity of *In Vitro* Evolved β-Glucuronidase. *J. Am. Chem. Soc.* **2014**, *136*, 5949−5955.
(24) Gorris, H. H.; Rissin, D. M.; Walt, D. R. Stochastic Inhibitor Release and Binding from Single-Enzyme Molecules. *Proc. Natl. Acad. Sci. U. S. A.* **2007**, *104*, 17680−17685.
(25) Chyan, W.; Raines, R. T. Enzyme-Activated Fluorogenic Probes for Live-Cell and *In Vivo* Imaging. *ACS Chem. Biol.* **2018**, *13*, 1810−1823.
(26) Komatsu, T.; Urano, Y. Evaluation of Enzymatic Activities in Living Systems with Small-Molecular Fluorescent Substrate Probes. *Anal. Sci.* **2015**, *31*, 257−265.
(27) Giacomini, K. M.; Huang, S. M.; Tweedie, D. J.; Benet, L. Z.; Brouwer, K. L.; Chu, X.; Dahlin, A.; Evers, R.; Fischer, V.; Hillgren, K. M.; Hoffmaster, K. A.; Ishikawa, T.; Keppler, D.; Kim, R. B.; Lee, C. A.; Niemi, M.; Polli, J. W.; Sugiyama, Y.; Swaan, P. W.; Ware, J. A.; et al. Membrane Transporters in Drug Development. *Nat. Rev. Drug Discovery* **2010**, *9*, 215−236.
(28) Watanabe, R.; Soga, N.; Fujita, D.; Tabata, K. V.; Yamauchi, L.; Kim, S. H.; Asanuma, D.; Kamiya, M.; Urano, Y.; Suga, H.; Noji, H. Arrayed Lipid Bilayer Chambers Allow Single-Molecule Analysis of Membrane Transporter Activity. *Nat. Commun.* **2014**, *5*, 4519.
(29) Watanabe, R.; Sakuragi, T.; Noji, H.; Nagata, S. Single-Molecule Analysis of Phospholipid Scrambling by TMEM16F. *Proc. Natl. Acad. Sci. U. S. A.* **2018**, *115*, 3066−3071.
(30) Zhang, Y.; Minagawa, Y.; Kizoe, H.; Miyazaki, K.; Iino, R.; Ueno, H.; Tabata, K. V.; Shimane, Y.; Noji, H. Accurate High-Throughput Screening Based on Digital Protein Synthesis in a Massively Parallel Femtoliter Droplet Array. *Sci. Adv.* **2019**, *5*, No. eaav8185.
(31) Tabata, K. V.; Sogo, T.; Moriizumi, Y.; Noji, H. Regeneration of *Escherichia Coli* Giant Protoplasts to Their Original Form. *Life* **2019**, *9*, 24.
(32) Visnapuu, M. L.; Duzdevich, D.; Greene, E. C. The Importance of Surfaces in Single-Molecule Bioscience. *Mol. BioSyst.* **2008**, *4*, 394−403.
(33) Galvagnion, C.; Buell, A. K.; Meisl, G.; Michaels, T. C.; Vendruscolo, M.; Knowles, T. P.; Dobson, C. M. Lipid Vesicles Trigger α-Synuclein Aggregation by Stimulating Primary Nucleation. *Nat. Chem. Biol.* **2015**, *11*, 229−234.
(34) Akbarzadeh, A.; Rezaei-Sadabady, R.; Davaran, S.; Joo, S. W.; Zarghami, N.; Hanifehpour, Y.; Samiei, M.; Kouhi, M.; Nejati-Koshki, K. Liposome: Classification, Preparation, and Applications. *Nanoscale Res. Lett.* **2013**, *8*, 102.
(35) Mayer, L. D.; Hope, M. J.; Cullis, P. R. Vesicles of Variable Sizes Produced by a Rapid Extrusion Procedure. *Biochim. Biophys. Acta, Biomembr.* **1986**, *858*, 161−168.
(36) van Swaay, D.; deMello, A. Microfluidic Methods for Forming Liposomes. *Lab Chip* **2013**, *13*, 752−767.
(37) Matosevic, S.; Paegel, B. M. Stepwise Synthesis of Giant Unilamellar Vesicles on a Microfluidic Assembly Line. *J. Am. Chem. Soc.* **2011**, *133*, 2798−2800.
(38) Deshpande, S.; Caspi, Y.; Meijering, A. E.; Dekker, C. Octanol-Assisted Liposome Assembly on Chip. *Nat. Commun.* **2016**, *7*, 10447.
(39) Deng, N. N.; Yelleswarapu, M.; Huck, W. T. Monodisperse Uni- and Multicompartment Liposomes. *J. Am. Chem. Soc.* **2016**, *138*, 7584−7591.
(40) Teh, S. Y.; Khnouf, R.; Fan, H.; Lee, A. P. Stable, Biocompatible Lipid Vesicle Generation by Solvent Extraction-Based Droplet Microfluidics. *Biomicrofluidics* **2011**, *5*, 44113.
(41) Arriaga, L. R.; Datta, S. S.; Kim, S. H.; Amstad, E.; Kodger, T. E.; Monroy, F.; Weitz, D. A. Ultrathin Shell Double Emulsion Templated Giant Unilamellar Lipid Vesicles with Controlled Microdomain Formation. *Small* **2014**, *10*, 950−956.
(42) Deshpande, S.; Spoelstra, W. K.; van Doorn, M.; Kerssemakers, J.; Dekker, C. Mechanical Division of Cell-Sized Liposomes. *ACS Nano* **2018**, *12*, 2560−2568.
(43) Ota, S.; Yoshizawa, S.; Takeuchi, S. Microfluidic Formation of Monodisperse, Cell-Sized, and Unilamellar Vesicles. *Angew. Chem., Int. Ed.* **2009**, *48*, 6533−6537.
(44) Soga, N.; Watanabe, R.; Noji, H. Attolitre-Sized Lipid Bilayer Chamber Array for Rapid Detection of Single Transporters. *Sci. Rep.* **2015**, *5*, 11025.
(45) Fukuyama, M.; Tokeshi, M.; Proskurnin, M. A.; Hibara, A. Dynamic Wettability of Polyethylene Glycol-Modified Poly(Dimethylsiloxane) Surfaces in an Aqueous/Organic Two-Phase System. *Lab Chip* **2018**, *18*, 356−361.
(46) Pautot, S.; Frisken, B. J.; Weitz, D. A. Production of Unilamellar Vesicles Using an Inverted Emulsion. *Langmuir* **2003**, *19*, 2870−2879.
(47) Chiba, M.; Miyazaki, M.; Ishiwata, S. Quantitative Analysis of the Lamellarity of Giant Liposomes Prepared by the Inverted Emulsion Method. *Biophys. J.* **2014**, *107*, 346−354.
(48) Noji, H.; Ueno, H.; McMillan, D. G. G. Catalytic Robustness and Torque Generation of the F_1-ATPase. *Biophys. Rev.* **2017**, *9*, 103−118.
(49) Asanuma, D.; Takaoka, Y.; Namiki, S.; Takikawa, K.; Kamiya, M.; Nagano, T.; Urano, Y.; Hirose, K. Acidic-Ph-Activatable Fluorescence Probes for Visualizing Exocytosis Dynamics. *Angew. Chem., Int. Ed.* **2014**, *53*, 6085−6089.
(50) Soga, N.; Kimura, K.; Kinosita, K., Jr.; Yoshida, M.; Suzuki, T. Perfect Chemomechanical Coupling of F_oF_1-ATP Synthase. *Proc. Natl. Acad. Sci. U. S. A.* **2017**, *114*, 4960−4965.
(51) Sunami, T.; Hosoda, K.; Suzuki, H.; Matsuura, T.; Yomo, T. Cellular Compartment Model for Exploring the Effect of the Lipidic Membrane on the Kinetics of Encapsulated Biochemical Reactions. *Langmuir* **2010**, *26*, 8544−8551.
(52) Nishimura, K.; Matsuura, T.; Nishimura, K.; Sunami, T.; Suzuki, H.; Yomo, T. Cell-Free Protein Synthesis inside Giant Unilamellar Vesicles Analyzed by Flow Cytometry. *Langmuir* **2012**, *28*, 8426−8432.

https://dx.doi.org/10.1021/acsnano.0c04354
ACS Nano 2020, 14, 11700−11711

(53) Harris, L. K.; Theriot, J. A. Surface Area to Volume Ratio: A Natural Variable for Bacterial Morphogenesis. *Trends Microbiol.* **2018**, *26*, 815−832.
(54) Sunami, T.; Ichihashi, N.; Nishikawa, T.; Kazuta, Y.; Yomo, T. Effect of Liposome Size on Internal RNA Replication Coupled with Replicase Translation. *ChemBioChem* **2016**, *17*, 1282−1289.
(55) Osawa, M.; Anderson, D. E.; Erickson, H. P. Reconstitution of Contractile FtsZ. Rings in Liposomes. *Science* **2008**, *320*, 792−794.
(56) Loose, M.; Fischer-Friedrich, E.; Ries, J.; Kruse, K.; Schwille, P. Spatial Regulators for Bacterial Cell Division Self-Organize into Surface Waves *In Vitro*. *Science* **2008**, *320*, 789−792.
(57) Bhattacharya, A.; Brea, R. J.; Niederholtmeyer, H.; Devaraj, N. K. A Minimal Biochemical Route towards *De Novo* Formation of Synthetic Phospholipid Membranes. *Nat. Commun.* **2019**, *10*, 300.
(58) Akama, K.; Iwanaga, N.; Yamawaki, K.; Okuda, M.; Jain, K.; Ueno, H.; Soga, N.; Minagawa, Y.; Noji, H. Wash- and Amplification-Free Digital Immunoassay Based on Single-Particle Motion Analysis. *ACS Nano* **2019**, *13*, 13116−13126.
(59) Okano, T.; Inoue, K.; Koseki, K.; Suzuki, H. Deformation Modes of Giant Unilamellar Vesicles Encapsulating Biopolymers. *ACS Synth. Biol.* **2018**, *7*, 739−747.
(60) Masaike, T.; Suzuki, T.; Tsunoda, S. P.; Konno, H.; Yoshida, M. Probing Conformations of the β Subunit of F_0F_1-ATP Synthase in Catalysis. *Biochem. Biophys. Res. Commun.* **2006**, *342*, 800−807.
(61) Soga, N.; Kinosita, K., Jr.; Yoshida, M.; Suzuki, T. Kinetic Equivalence of Transmembrane pH and Electrical Potential Differences in ATP Synthesis. *J. Biol. Chem.* **2012**, *287*, 9633−9639.
(62) Shimizu, Y.; Inoue, A.; Tomari, Y.; Suzuki, T.; Yokogawa, T.; Nishikawa, K.; Ueda, T. Cell-Free Translation Reconstituted with Purified Components. *Nat. Biotechnol.* **2001**, *19*, 751−755.

https://dx.doi.org/10.1021/acsnano.0c04354
ACS Nano 2020, 14, 11700−11711